

Microscopy Image Restoration with Deep Wiener-Kolmogorov Filters

Valeriya Pronina¹, Filippos Kokkinos², Dmitry V. Dyllov¹, and Stamatios Lefkimmiatis³

¹Skolkovo Institute of Science and Technology, Moscow, Russia

²University College London

³Q.bio Inc.

Abstract

Microscopy is a powerful visualization tool in biology, enabling the study of cells, tissues, and the fundamental biological processes. Yet, the observed images of the objects at the micro-scale suffer from two major inherent distortions: the blur caused by the diffraction of light, and the background noise caused by the imperfections of the imaging detectors. The latter is especially severe in fluorescence and in confocal microscopes, which are known for operating at the low photon count with the Poisson noise statistics. Restoration of such images is usually accomplished by image deconvolution, with the nature of the noise statistics taken into account, and by solving an optimization problem given some prior information about the underlying data (i.e., regularization). In this work, we propose a unifying framework of algorithms for Poisson image deblurring and denoising. The algorithms are based on deep learning techniques for the design of learnable regularizers paired with an appropriate optimization scheme. Our extensive experimentation line showcases that the proposed approach achieves superior quality of image reconstruction and beats the solutions that rely on deep learning or on the optimization schemes alone. Moreover, several implementations of the proposed framework demonstrate competitive performance at a low computational complexity, which is of high importance for real-time imaging applications.

1. Introduction

Microscopes are widely used in biological and medical research, allowing the study of organic and inorganic substances at the minuscule scale. The observed microscopy images, however, suffer from the following two inherent distortions: a blur of detail caused by the resolution limit of a microscope, and a background noise introduced by the imperfections of the imaging system as a whole and by the image-recording sensor in particular. Both of these traits not only distort the perception of the detail in the im-

age, but also influence the quantitative analysis of its content [12, 13].

Mathematically, the image formation process can be described by the operation of convolution, where the underlying image is convolved with the point spread function of the microscope [42, 16]. The image is then corrupted by shot noise during the photon detection process in the imaging detector of the microscope, e.g., in the photomultiplier tube or in the charge coupled device. Two imaging systems – fluorescent and confocal microscopes – are very popular among biologists and are especially prone to the high shot noise. If the number of photons captured by these modalities is rather small, the underlying statistics of the noise becomes Poisson, giving the image a distinctively displeasing look and complicating its consequent analysis.

Restoration of photon-limited microscopy images is an ill-posed inverse problem where a unique solution does not exist [16]. One, therefore, needs to constrain the space of solutions in order to obtain a statistically or a physically meaningful one. A popular approach for doing that follows the variational formulation of the problem, where the restored image is obtained as the minimizer of an objective function [2]. This function comprises two terms: the data fidelity term that measures the proximity between the obtained measurements and the solution, and the regularization term that integrates prior information about the expected solution. There are several methods focused on the development of an effective regularization scheme for the image restoration, e.g., the Hyper-Laplacian priors [22], the non-local means [8], the shrinkage fields [41], and others.

With the advent of deep learning, many inverse problems have been successfully approached with Fully Convolutional Neural Networks (FCNNs) [35, 44] which can learn a mapping between the measured image and its expected reconstruction. Furthermore, a series of works have incorporated deep learning for the regularization purposes in a wide range of image restoration problems [50, 25, 26, 51, 23, 20]. Such a regularization paradigm, in turn, has allowed to sur-

pass the performance of the one-shot methods relying on FCNNs. However, none of these techniques has been applied to the Poisson deblurring problem.

In this work, we present a new Poisson deblurring framework comprising a collection of methods that leverage the advantages of both the classical schemes for optimization, and the deep learning approaches for regularization. We develop an extensive set of techniques for handling the image prior information, by using both shallow and deep learning for parametrization. The proposed framework entails the following steps:

- First, a regularizer is formed as a group of learnable kernels and is deployed to every image identically.
- Second, an intuitive extension is further examined with the group of kernels being predicted *per image* using a compact FCNN as a Kernel Prediction Network (KPN).
- The same kernel-predicting approach is then probed in *per pixel* evaluation, with the KPN predicting the appropriate regularizer for each spatial location in the image.
- The last step consists of approximating the entire regularization function with a neural network, which is then employed in an iterative manner.

The developed methods outperform solutions based either on optimization schemes alone or the solutions based merely on deep learning techniques. Exploiting both the classical optimization and the deep learning methodologies, the proposed approaches are intrinsically ready for fine-tuning the trade-off between the computational efficiency and the accuracy of image reconstruction.

2. Related work

Deconvolution in the presence of Poisson noise is generally considered a challenging task, and it has attracted significant attention by the research community. Several attempts have been made to develop an optimal approach according to some criterion. One of the most well-known classical methods is the Richardson-Lucy (RL) algorithm that retrieves the maximum-likelihood estimate of the distorted signal under the assumption of Poisson noise statistics [31, 38]. The main drawback of RL is the amplification of the noise after a small number of iterations due to the algorithm's intrinsic multiplicative update rule, which does not always converge to a solution.

To address this problem, many researchers have resorted to hand-crafted regularization schemes in order to drive the solution of the optimization problem towards a subset of physically plausible image reconstructions. The regularization in [14, 24] relied on the total-variation regularization (TV), whereas the scheme in [9, 28] considers wavelet-based regularization to deal with the problem of

Poisson image deblurring. Few authors have also suggested modifications of the original RL algorithm to accelerate its rate of convergence [47, 37]. Moreover, Lefkimmiatis and Unser developed a highly efficient method using the Hessian Schatten-norm regularization for Poisson log-likelihood estimation [27]. Another line of algorithms is based on the alternating direction method of multipliers (ADMM), proposed in [17] to perform deconvolution in the presence of Poisson noise. In [10], an accelerated linearized alternating minimization allowed to outperform ADMM, while combining it with the TV regularization [32] proved efficient for the deblurring task.

The Wiener-Kolmogorov filter, or Wiener filter, is another classical solution for image deblurring and denoising [48, 19]. This method retrieves the minimum mean squared error estimate and it has established itself as a fast deconvolution algorithm [4, 7, 52] due to the closed-form solution in the Fourier domain. However, it is derived under the assumption of Gaussian noise, and thus, its performance is mediocre when applied to data obeying the Poisson distribution. One common way to ameliorate this deficiency is to first apply a variance stabilizing transformation (VST) [34] which transforms a variable from the Poisson distribution into one from the Gaussian. This allows to borrow the ample apparatus of the well-studied methods derived for Gaussian statistics. This approach was successfully used in [34, 18, 53] to solve the Poissonian restoration problem using Gaussian denoising algorithms. Additionally, Lu *et al.* in [30] deployed VST to reduce the Poisson noise in spectral imaging problems using the Wiener filter. More recently, the Wiener filter became a part of methods such as PURE-LET [28] and SURE-LET [52], performing deconvolution with a piece-wise thresholding under wavelet coefficients regularization.

Being widely used in many research areas, including the biomedical field, a plethora of neural network approaches have been proposed for denoising [35], demosaicking [21], and super-resolution [44]. Deep learning methods are also applied in image deblurring, e.g., in [15], where a CNN is used for restoring images corrupted with various visual artifacts, and in [11], where a parametric CNN model was used to enhance a shape-based artifact elimination. Liu and Lam in [29] proposed a neural network for Poisson image denoising, and in [49] the authors proposed a CNN that learns the deconvolution operation for natural images in a supervised manner. A step into combining traditional optimization schemes with deep learning is made in [36] where a basic deconvolution algorithm was boosted by a CNN. Finally, Kruse *et al.* [23] developed an iterative FFT-based deconvolution approach using a learnable regularization via CNNs that mathematically resembles an iterative Wiener Filter.

3. Problem formulation

3.1. Image formation in photon-limited microscopy

The image formation process can be described by the observation model

$$\mathbf{y} = \mathcal{P}(\mathbf{K}\mathbf{x}), \quad (1)$$

where $\mathbf{y} \in \mathbb{R}^N$ corresponds to the observed image, $\mathbf{K} \in \mathbb{R}^{N \times N}$ is the matrix corresponding to the point spread function (PSF), $\mathbf{x} \in \mathbb{R}^N$ is the underlying image that we aim to restore and \mathcal{P} denotes the Poisson noise distorting the image. While \mathbf{x} and \mathbf{y} are two dimensional images, for the sake of mathematical derivations, we assume that they have been raster scanned using a lexicographical order, and they correspond to vectors of N dimensions.

The deconvolution problem of photon-limited microscopy is to estimate the underlying ground-truth image \mathbf{x} from the distorted measurement \mathbf{y} in the presence of Poisson, or shot, noise. One notable property of the Poisson distribution is that the mean and variance of a signal are not independent, i.e. $\text{mean}(\mathbf{y}) = \text{var}(\mathbf{y})$. To transform a variable that follows the Poisson distribution into one that follows a standard Gaussian distribution, we make use of the widely known VST algorithm, the Anscombe transform [5], which is applied on the distorted observation

$$\mathbf{y} \rightarrow 2\sqrt{\mathbf{y} + \frac{3}{8}}. \quad (2)$$

Anscombe transform aims to stabilize the data variance to be approximately unity. After the transformation, the data can be viewed as a signal-independent Gaussian process with unity variance and zero mean, and therefore a method derived from Gaussian statistics can be successfully applied for solving a restoration problem. One example of such a method is the Wiener-Kolmogorov filter, which is historically considered an effective deconvolution method. Once the deconvolved solution, denoted as $\hat{\mathbf{x}}$, is obtained, an inverse Anscombe transform is applied to return the data to its original domain. Applying the simple algebraic inverse usually results in a biased estimate of the output. To mitigate the bias in the case of photon-limited imaging the exact unbiased inverse transformation should be used, whose closed-form approximation [33] is

$$\hat{\mathbf{x}} \rightarrow \left(\frac{\hat{\mathbf{x}}}{2}\right)^2 - \frac{1}{8} + \frac{1}{4}\sqrt{\frac{3}{2}}\hat{\mathbf{x}}^{-1} - \frac{11}{8}\hat{\mathbf{x}}^{-2} + \frac{5}{8}\sqrt{\frac{3}{2}}\hat{\mathbf{x}}^{-3}. \quad (3)$$

In our work, the Anscombe transform is applied on the input image \mathbf{y} as described in Eq. (2) before being fed into any of the proposed models in Section 4. Accordingly, we assume that the restored signal $\hat{\mathbf{x}}$ of any model is transformed back using the exact unbiased version of the inverse transformation, presented in Eq. (3), and thus the final restored image is obtained.

3.2. Regularization

Deconvolution being an image restoration task is an ill-posed inverse problem, which implies that a unique solution does not exist. Therefore the goal here is out of the infinity of existing solutions to compute a meaningful one that exhibits certain properties. In general, such problems can be addressed following a variational approach whose solution $\hat{\mathbf{x}}$ can be obtained by minimizing the objective function,

$$\hat{\mathbf{x}} = \underset{\mathbf{x}}{\text{argmin}} \underbrace{\frac{1}{2}\|\mathbf{y} - \mathbf{K}\mathbf{x}\|_2^2}_{\mathcal{J}(\mathbf{x})} + \lambda r(\mathbf{x}). \quad (4)$$

Here the first term corresponds to the data fidelity term, which measures the proximity of the solution to the observation, while the second one corresponds to the regularizer that models any prior knowledge one might have about the ground-truth image. The parameter λ is a trade-off coefficient that determines the contribution of the regularizer into the estimation of the solution. A list of popular regularizers contains Tikhonov [45] and TV functionals [39] which have been widely used in a plethora of image restoration tasks, including deconvolution problems [14]. However, in this work we attempt to incorporate prior information learned directly from available training data in a supervised manner with the inclusion of deep learning strategies.

4. Proposed approach

4.1. Learnable regularization kernels

First, we start from the observation that in most of the modern methods for image restoration the regularization term is formed as

$$r(\mathbf{x}) = \sum_{d=1}^D \rho_d(\mathbf{g}_d * \mathbf{x}), \quad (5)$$

where \mathbf{g}_d are typically linear filters and $\rho_d(\cdot)$ is a set of penalty functions, acting on the filters outputs [22]. In this work, we explicitly set the penalty function to be the squared ℓ_2 norm, leading to a Tikhonov regularizer [45]

$$r(\mathbf{x}) = \sum_{d=1}^D \|\mathbf{g}_d * \mathbf{x}\|_2^2 = \sum_{d=1}^D \|\mathbf{G}_d \mathbf{x}\|_2^2, \quad (6)$$

where \mathbf{g}_d are learnable convolution kernels and $\mathbf{G}_d \in \mathbb{R}^{N \times N}$ are convolution matrices, corresponding to these kernels. This specific choice of the penalty function allows us to obtain the solution of (4) in the closed-form

$$\hat{\mathbf{x}} = (\mathbf{K}^\top \mathbf{K} + \lambda \sum_{d=1}^D \mathbf{G}_d^\top \mathbf{G}_d)^{-1} \mathbf{K}^\top \mathbf{y}, \quad (7)$$

which corresponds to the Wiener-Kolmogorov filter. Here \mathbf{K}^\top and \mathbf{G}_d^\top are the adjoint matrices of \mathbf{K} and \mathbf{G}_d , respectively. In order to obtain the solution of Eq. (7) one has

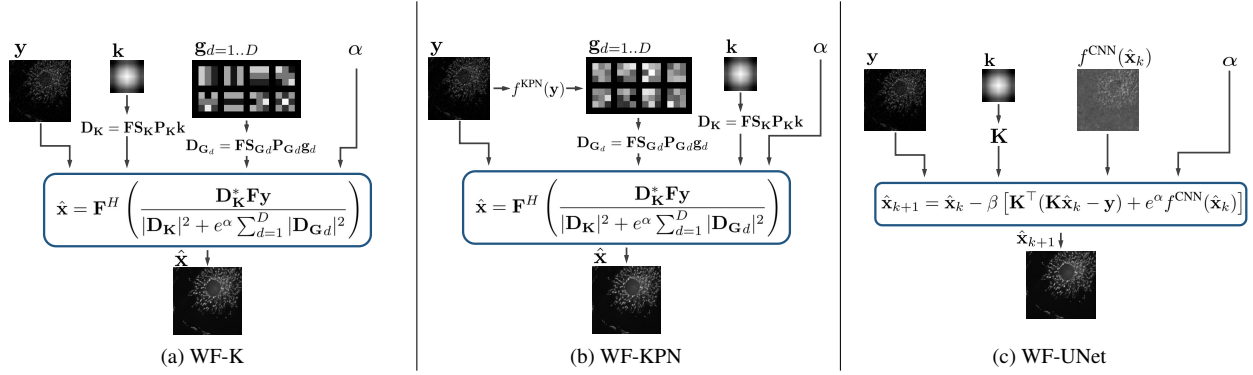


Figure 1: Overview of the three main proposed prior parametrization models. In Fig. 1a the one-shot Wiener filter with learnable kernels is depicted, while in 1b the same filter with predictable kernels is presented. The proposed iterative scheme which combines Wiener filtering with the approximation of regularization with a CNN is visualized in 1c. For visualization purposes, we exclude the Anscombe transform that is applied on the observed signal as well as the inverse transformation which is applied on the predicted underlying image.

first to perform the inversion of a huge matrix which can be very slow in practice or even intractable. However, the supremacy of the Wiener filter lies in its FFT-based inference, which renders it a fast and efficient method and allows to restore the underlying signal at a low computational complexity. Specifically, under the assumption of periodic image boundary conditions, the degradation matrix \mathbf{K} and convolution matrix \mathbf{G}_d are circulant real matrices, therefore they can be diagonalized in the Fourier domain as

$$\mathbf{K} = \mathbf{F}^H \mathbf{D}_{\mathbf{K}} \mathbf{F}, \quad \mathbf{G}_d = \mathbf{F}^H \mathbf{D}_{\mathbf{G}_d} \mathbf{F} \quad (8)$$

$$\mathbf{D}_{\mathbf{K}} = \mathbf{F} \mathbf{S}_{\mathbf{K}} \mathbf{P}_{\mathbf{K}} \mathbf{k}, \quad \mathbf{D}_{\mathbf{G}_d} = \mathbf{F} \mathbf{S}_{\mathbf{G}_d} \mathbf{P}_{\mathbf{G}_d} \mathbf{g}_d. \quad (9)$$

Here $\mathbf{F} \in \mathbb{C}^{N \times N}$ is the Fourier (DFT) matrix, $\mathbf{F}^H \in \mathbb{C}^{N \times N}$ is its inverse, $\mathbf{D}_{\mathbf{K}}, \mathbf{D}_{\mathbf{G}_d} \in \mathbb{C}^{N \times N}$ are diagonal matrices, $\mathbf{S}_{\mathbf{K}}, \mathbf{S}_{\mathbf{G}_d} \in \mathbb{R}^{N \times N}$ are the corresponding circulant shift operators, $\mathbf{P}_{\mathbf{K}} \in \mathbb{R}^{N \times M}$, $\mathbf{P}_{\mathbf{G}_d} \in \mathbb{R}^{N \times L_d}$ are the corresponding zero-padding operators, $\mathbf{k} \in \mathbb{R}^M$ is the blurring kernel and $\mathbf{g}_d \in \mathbb{R}^{L_d}$ is a regularization convolution kernel. We also consider the trade-off coefficient λ to be equal to e^α in all experiments to ensure the positivity of the regularization weight. Based on the above, the one-shot solution of Eq. (7) is

$$\hat{\mathbf{x}} = \mathbf{F}^H \left(\frac{\mathbf{D}_{\mathbf{K}}^* \mathbf{F} \mathbf{y}}{|\mathbf{D}_{\mathbf{K}}|^2 + e^\alpha \sum_{d=1}^D |\mathbf{D}_{\mathbf{G}_d}|^2} \right), \quad (10)$$

where $\mathbf{D}_{\mathbf{K}}^*$ is conjugate to $\mathbf{D}_{\mathbf{K}}$. The method is depicted in Fig. 1a and hereafter we refer to it as WF-K. To obtain the solution in this form, we firstly employ a group of D learnable kernels \mathbf{g}_d of size $K \times K$ which are initialized using a two-dimensional discrete cosine transform (DCT) frequency basis; a common choice in image processing since it has shown the ability to extract useful prior image information. We also consider α to be a learnable parameter in all proposed regularization schemes in order for the trade-off

coefficient value to be tuned alongside the learnable kernels during the training process.

4.2. Prediction of regularization kernels

A critical drawback of the WF-K method lies in the way the group of kernels is formulated. In detail, the learnable group is global which means that all kernels are applied on every image identically without any dependency on the depicted content. To remedy this situation, we propose the content-driven WF-KPN method that predicts per image the group of kernels that need to be used for regularization. In this framework, the solution of a Wiener filter yields the same form as presented in Eq. (10), but unlike the previous approach, the convolution kernels \mathbf{g}_d , that form the diagonal matrix $\mathbf{D}_{\mathbf{G}_d}$ in Eq. (9), are now predicted from the Kernel Prediction Network (KPN) [35] as shown in Fig. 1b. We further refer to this method as WF-KPN.

For the Kernel Prediction Network we select a compact UNet architecture with nearly 470k parameters that receives the distorted input \mathbf{y} and produces an output with $K^2 D$ channels and the same spatial resolution as the input. Unlike the traditional UNet, we perform global average pooling in the spatial dimension on the output of the last layer, which is then reshaped into a stack of $D \times K \times K$ regularization kernels. Here D is the number of kernels and $K \times K$ is the support size. In all our experiments, we set $D = 8$ and $K = 3$. We also use instance normalization [46] after each convolutional layer to normalize weights for each image independently. In this way, the KPN predicts D content dependent regularization kernels of size $K \times K$ for each image, that then under the assumption of periodic boundary conditions form the diagonal matrix $\mathbf{D}_{\mathbf{G}_d}$ in Eq. (9). After that, the resulting diagonal matrices $\mathbf{D}_{\mathbf{G}_d}$ are incorporated into the solution of the Wiener filter according to Eq. (10).

The proposed models WF-K and WF-KPN assume

learning of the trade-off coefficient α and regularization kernels \mathbf{g}_d in a supervised manner via means of a gradient-based minimization of a loss function. To efficiently calculate gradients of the loss function and update the learnable parameters of the model, one commonly used algorithm is backpropagation. With modern tools, it is possible to perform backpropagation with automatically built computational graphs. However, the closed-form solution in Eq. (10) involves complex functions and operations that cannot be calculated using automatic differentiation.

To overcome this issue, one can perform direct differentiation of the solution $\hat{\mathbf{x}}$ w.r.t. the learnable parameters. This way the differentiation of a real-valued function w.r.t. the real-valued parameters is performed, allowing to avoid differentiation of non-analytic functions.

4.3. Prediction of spatially adaptive regularization kernels

While the prediction of global regularization kernels per image provides the appealing property of content adaptation, we further extend WF-KPN to be both spatially and content adaptive. This is achieved by predicting for each image a different regularization kernel per-pixel for an image and hence the method is dubbed as WF-KPN-SA. For this extension, we modify the UNet of Section 4.2 to predict a kernel per spatial location of an image. Unlike WF-KPN, the output of the network has K^2 channels and the same size as the input. We empirically found that normalization of the network hinders the performance and therefore it was removed in all WF-KPN-SA related experiments. Furthermore, the output of the network is reshaped into spatially adaptive regularization kernels of size $K \times K$ for each pixel of an input image. These kernels are then unfolded into a matrix \mathbf{G} which now does not correspond to a circulant matrix, and, thus, the FFT-based inference of the Wiener-Kolmogorov filter is not feasible. The solution of the restoration problem has now the form of

$$\hat{\mathbf{x}} = (\mathbf{K}^\top \mathbf{K} + e^\alpha \mathbf{G}^\top \mathbf{G})^{-1} \mathbf{K}^\top \mathbf{y} \quad (11)$$

and the calculation of $\hat{\mathbf{x}}$ is done using the conjugate gradient algorithm [43].

4.4. Prediction of the gradient of the regularizer

Finally, with the desire to fully exploit deep learning capabilities, we employ a CNN for parametrizing a prior that would be specific for each image and, thus, completely content adaptive. This way we do not make assumptions about the form of the regularization term, therefore the solution of Eq. (4) cannot be derived with a closed-form expression. One common way to solve Eq. (4) in this case is to apply gradient descent [6] optimization algorithm to find a solution that ensures the minimum of an objective function $\mathbf{J}(\mathbf{x})$,

$$\hat{\mathbf{x}}_{k+1} = \hat{\mathbf{x}}_k - \beta \nabla \mathbf{J}(\mathbf{x}). \quad (12)$$

Here $\hat{\mathbf{x}}_{k+1}$ is the solution of Eq. (4) that is updated after each iteration k of the gradient descent scheme and β is the learning rate defining the speed of the algorithm. Introducing the objective function $\mathbf{J}(\mathbf{x})$, defined according to Eq. (4), into Eq. (12), we obtain the solution of the gradient descent scheme,

$$\hat{\mathbf{x}}_{k+1} = \hat{\mathbf{x}}_k - \beta [\mathbf{K}^\top (\mathbf{K} \hat{\mathbf{x}}_k - \mathbf{y}) + e^\alpha f^{\text{CNN}}(\hat{\mathbf{x}}_k)]. \quad (13)$$

Here we parametrize the gradient of the regularizer with the CNN, $\nabla \mathbf{r}(\hat{\mathbf{x}}_k) = f^{\text{CNN}}(\hat{\mathbf{x}}_k)$. For the prediction of the gradient of a regularizer we employ the UNet architecture that was defined in Section 4.2. Unlike WF-KPN and WF-KPN-SA, we do not modify the original UNet architecture, and in this case the network receives a distorted image \mathbf{y} as an input and maps it to an output with the same resolution and number of channels as the input. We also use instance normalization after each convolutional layer to normalize weights for each image independently. With a slight abuse of notation, the method is hereafter referred as WF-UNet and it is depicted in Fig. 1c. The number of gradient descent iterations for WF-UNet is set to be equal to 10. We also consider the step size β to be a learnable parameter in order for the gradient descent speed to be tuned during the training process.

We stress that the proposed methods, WF-KPN, WF-KPN-SA and WF-UNet, share a UNet with almost identical architecture in order to have approximately the same number of trainable parameters that allows for fair comparison between the models. Furthermore, the selected network architecture is relatively compact, which in return allows the development of methods capable of deblurring an image in milliseconds.

5. Network training

5.1. Dataset

Since there is a lack of a Poisson noise perturbed deconvolution dataset, comprising of microscopy images, we create training pairs of ground-truth and distorted with blur and Poisson noise images using the Fluorescence Microscopy Denoising (FMD) dataset [53] and a dataset that is used in cell segmentation of microscopy images [3]. To create a large set of reference images, we take the ground-truth images from both datasets and crop each image into patches of size 256×256 . Consequently, all patches that contain no information about cells are discarded by comparing the mean value of a patch with the mean value of the original image. Note that all ground-truth images as well as resulting distorted images are grayscale.

To produce blurred versions of the ground-truth images we create 35 different 2D PSFs of size 5×5 by altering index of refraction of the media, numerical aperture and excitation wavelength using the ImageJ plugin Diffraction PSF 3D [1]. In detail, 25 PSFs are reserved for training,

	PEAK											
	1		2		5		10		25		50	
	PSNR	SSIM	PSNR	SSIM	PSNR	SSIM	PSNR	SSIM	PSNR	SSIM	PSNR	SSIM
Input	10.94	.0985	13.23	.1113	16.68	.1654	19.47	.2450	23.25	.3968	26.06	.5294
RLTV [14]	12.40	.1021	12.61	.1048	13.75	.1240	15.72	.1564	19.24	.2391	22.32	.3435
PIDAL [17]	25.57	.5229	26.69	.5625	25.78	.4831	28.34	.6081	30.61	.7135	31.31	.7533
GILAM [10]	24.44	.4867	25.62	.6259	26.53	.5356	28.16	.6229	29.86	.6917	31.04	.7413
PURE-LET [28]	26.19	.7357	26.45	.7508	26.77	.7615	27.65	.7795	28.75	.8063	28.77	.8117
HSPiRAL [27]	22.98	.3952	26.39	.5694	30.13	.7537	31.98	.8232	33.51	.8604	33.83	.8586
UNet	28.73	.7969	29.89	.8188	31.46	.8479	32.67	.8680	34.12	.8912	35.18	.9057
WF-K	25.30	.5250	27.74	.6085	28.85	.6894	28.80	.7268	28.71	.7526	28.65	.7618
WF-KPN	27.18	.7512	28.43	.7593	29.41	.7618	29.94	.7697	30.61	.7840	30.99	.7939
WF-KPN-SA	28.73	.7880	30.04	.8143	31.75	.8476	33.06	.8700	34.65	.8953	35.81	.9103
WF-UNet	28.91	.8013	30.13	.8233	31.74	.8520	32.98	.8723	34.50	.8955	35.56	.9098

Table 1: PSNR and SSIM comparisons on Poisson image deblurring for six different noise levels.

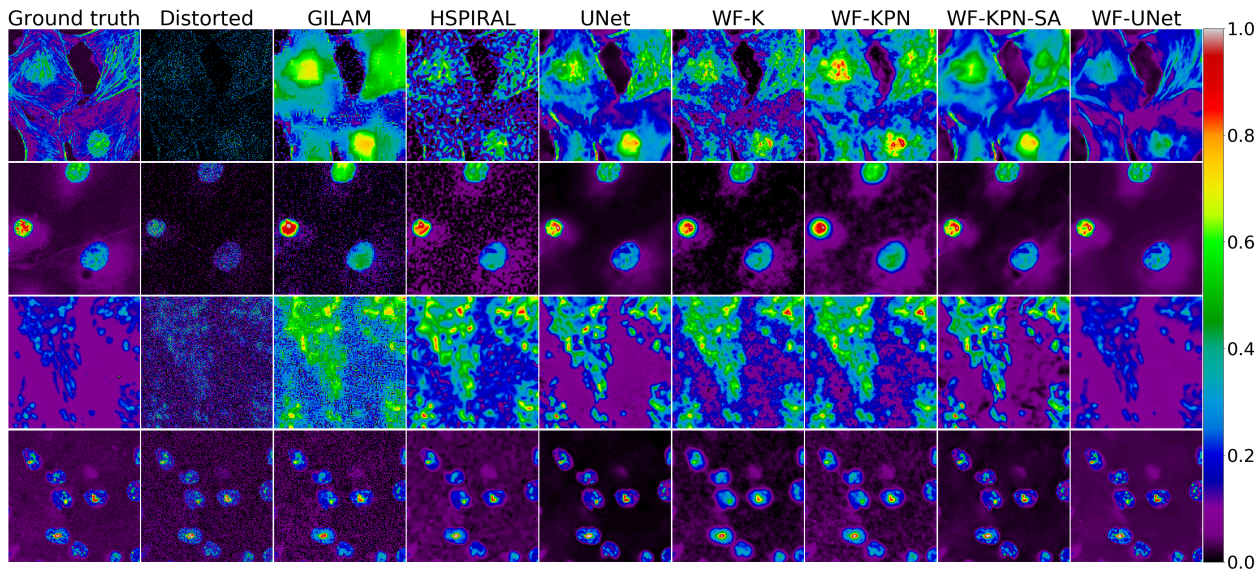


Figure 2: Restoration of the microscopy images scaled to maximum intensities peak equal to 1, 5, 10, 25 from top to bottom and degraded by PSF and Poisson noise. All images are originally grayscale, but we used a different colormap to stress the differences in details of image structures.

5 for validation and the rest for testing purposes. Notably, all PSFs k are normalized such that $\sum_i k_i = 1$, which is a realistic assumption in optics [14]. To simulate various SNR values of Poisson noise, we use the prior art approach [10, 27] and scale the ground-truth images to have a maximum intensity of (1, 2, 5, 10, 25, 50). Poisson noise is signal dependent with local $\text{SNR} = \sqrt{y_i}$, where y_i denotes the underlying image intensity at position i , therefore by increasing the maximum intensity of an image, the amount of noise decreases and vice versa. Furthermore, it is long known fact that images with large mean value and perturbed with Poisson noise follow approximately a normal, or Gaussian distribution, and therefore methods based on Gaussian statistics might work equally well. Scaling the ground-truth images to have various ranges of maximum intensities aims to cover a wide gamut of noise levels, including the ones that belong to approximately a Gaussian distribution.

The resulting dataset, which contains 1405 pairs of ground-truth and distorted images, is split into 975 training, 200 validation and 230 testing samples. During training, a ground-truth sample is rescaled to a randomly chosen maximum intensity from the range mentioned above, then convolved with a randomly chosen blur kernel from the 25 training PSFs, and after that the noisy observation is produced from the blurred image. We also implement data augmentation during training with random vertical and horizontal flips as well as random horizontal shifts all of which are realistic in practice.

5.2. Training details

All proposed methods are trained end-to-end to minimize the ℓ_1 loss function between the output and the ground-truth image as well as the gradients of the afore-

	STD									
	0.001		0.005		0.01		0.05		0.1	
	PSNR	SSIM	PSNR	SSIM	PSNR	SSIM	PSNR	SSIM	PSNR	SSIM
Input	41.69	.9595	39.62	.9428	36.99	.8968	26.68	.4304	21.39	.1979
ICRNN [51]	39.65	.9446	39.84	.9451	39.71	.9436	34.76	.8385	30.59	.7376
UNet	41.85	.9676	40.58	.9604	39.51	.9506	35.57	.8988	33.20	.8367
WF-K	38.82	.9296	38.69	.9278	38.32	.9222	33.96	.8187	29.60	.6762
WF-KPN	43.81	.9738	41.89	.9638	40.12	.9487	33.48	.8381	29.31	.7554
WF-KPN-SA	44.28	.9753	42.28	.9656	40.60	.9499	34.76	.8417	30.80	.7460
WF-UNet	43.04	.9684	41.91	.9613	40.61	.9510	36.15	.8972	33.74	.8522

Table 2: PSNR and SSIM comparisons on Gaussian image deblurring for five noise levels.

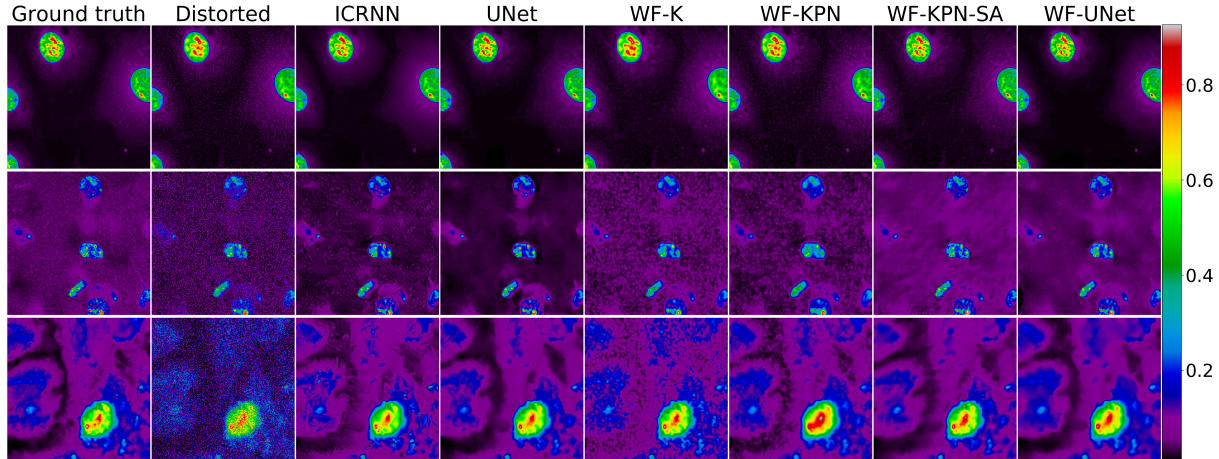


Figure 3: Restoration of the microscopy images degraded by PSF and Gaussian noise with standard deviation equal to 0.01, 0.05, 0.1 from top to bottom. All images are originally grayscale but we use a different colormap to stress the differences in details of image structures.

mentioned entities

$$\mathcal{L} = \|\hat{\mathbf{x}} - \mathbf{x}\|_1 + \|\nabla\hat{\mathbf{x}} - \nabla\mathbf{x}\|_1. \quad (14)$$

By incorporating a gradient based loss alongside the pixel-wise loss, we obtain models that are capable of reconstructing the sharp details. All proposed methods are optimized using Adam with learning rate 10^{-3} . For all methods, except the WF-KPN-SA, we use batch size equal to 25 and train model for 300 epochs. Due to memory restrictions, we set the batch size to be equal to 3 for the method WF-KPN-SA.

5.3. Evaluation

To evaluate the performance of all algorithms on each noise level, we use 230 ground-truth images and rescale them to each value from the (1, 2, 5, 10, 25, 50) range. Afterwards, we convolve the rescaled ground-truth image with a fixed blur kernel from the 5 PSFs reserved for testing purposes. Note that the held-out PSFs were not seen during training in order to explore the generalization ability of the methods to unknown blurring kernels. Finally, the noisy observation of a blurry image is produced. In detail, we get 1380 test samples in total, combined into 6 test sets of dif-

ferent noise levels which allows the thorough comparison of the performance of our algorithms on each noise level separately.

We compare the proposed algorithms with the non-blind deblurring algorithms, developed for Poisson distribution: RLTV [14, 40], PIDAL [17], GILAM [10], HSPIRAL[27] and PURE-LET [28]. For each of these methods, we use the parameters suggested in the literature. We also build a CNN baseline which is a UNet architecture with the same number of parameters as the one used for parametrization of the regularization gradient. This way we get a valid comparison and are able to see if the combination of a standard optimization scheme and a deep learning approach for a priori information about the expected solution will help to achieve good restoration results and overcome pure optimization scheme and solely deep learning based algorithm. For assessing the methods performance we use the standard peak signal-to-noise ratio (PSNR) and structural similarity index (SSIM) metrics.

6. Results

We evaluate all methods on the developed test set across all different noise ranges, as described in Section 5.3. The

results presented in Table 1 and Table 3 show that the first proposed method based on learning of regularization kernels, WF-K, is not only very competitive against the previous state-of-the-art methods, but also superior in terms of runtime. Notably, WF-K shows higher requirement of computational time on GPU due to a large number of FFT-based operations. However, this method achieves better quantitative results than the previous state-of-the-art methods on the intensity peaks below 5, being marginally inferior only to PIDAL and PURE-LET. Nonetheless, the other regularization schemes proposed herein, although slower in terms of runtime than WF-K, achieve significantly better results both in terms of metrics and in terms of visual perception at a low computational complexity, with only WF-KPN-SA and WF-UNet being slower than PURE-LET on CPU. Comparison of the runtimes was conducted on Intel Core i7-8750H CPU and NVIDIA GeForce GTX 1080Ti.

Table 1 and Fig. 2 clearly show that WF-UNet outperforms the other approaches at most the noise levels, which is especially important on the low intensity peak values where the Poisson noise is stronger. WF-KPN-SA and WF-UNet show comparable performance on higher intensity peaks, with WF-KPN-SA achieving slightly better results on the highest peak. Overall, WF-UNet and WF-KPN-SA show good quantitative improvement from nearly 1.5dB to 3.5dB over the previous state-of-the-art methods on the low intensity peaks and from 1dB to 2dB on the high intensity peaks. Moreover, Fig. 2 demonstrates that, despite the good quantitative improvement, WF-K and WF-KPN struggle to reconstruct the fine details in the images, while the reconstructions generated by WF-KPN-SA and WF-UNet methods are very accurate.

6.1. Deblurring under Gaussian noise

The Wiener-Kolmogorov filter was originally designed under the assumption of Gaussian noise, therefore a natural ablation study is to apply the proposed algorithms for im-

	CPU, ms	GPU, ms
RLTV [40]	2385.9	–
PIDAL [17]	5680.9	–
GILAM [10]	4155.9	–
HSPiRAL [27]	5828.8	–
PURE-LET [28]	211.3	–
UNet	32.4	2.8
WF-K	5.6	4.6
WF-KPN	48.7	5.7
WF-KPN-SA	968.2	341.4
WF-UNet	354.1	45.5

Table 3: Runtime of several deconvolution algorithms for processing an image with spatial dimension equal to 256×256 . All times were calculated using the publicly available implementations and the reported benchmarks are the average of 10 runs.

age deblurring under Gaussian noise. Gaussian denoising and deblurring is still an open issue, and there is a plethora of methods that have been proposed, including the ones that combine deep learning methods and standard optimization schemes [23, 51, 50]. We compare our proposed algorithms with one state-of-the-art algorithm for deblurring images distorted with Gaussian noise – ICRNN [51]. For evaluating this method, we use the parameters suggested in the original publication and the accompanied software.

To assess the performance of our algorithms on the task of deblurring images corrupted by Gaussian noise, we use the same dataset as the one used for the evaluation of the Poisson deblurring. All images are scaled in the range of $[0, 1]$, then blurred with a PSF and finally perturbed with iid Gaussian noise with standard deviation from the set $(0.001, 0.005, 0.01, 0.05, 0.1)$. The training pipeline is the same as the one explained in Section 5.1, and we follow the same logic as in Section 5.3 for producing blurred and noisy observations for the test set.

From the deconvolution results, presented in Table 2 and Fig. 3, it is clear that WF-UNet outperforms other methods both in terms of metrics and visual quality and is only comparable with WF-KPN and inferior to WF-KPN-SA on the lower noise levels, where WF-KPN-SA achieves superior results. As presented in Fig. 3, WF-K and WF-KPN methods tend to miss sharp details in the restored images, while WF-KPN-SA and WF-UNet allow the restoration of fine image details and have a good quantitative improvement from nearly 2.5dB to 4.5dB for WF-KPN-SA on low noise levels and from 0.9dB to nearly 3dB for WF-UNet on higher noise levels over the state-of-the-art algorithm.

7. Conclusion

In this work, we proposed a series of methods based on the Wiener-Kolmogorov filtering technique for treating the problem of Poisson image deblurring and denoising. We introduced three ways to parametrize the image priors including a new approach of regularization with the kernel predictions via a neural network. Our extensive experimentation line showcased that the proposed framework of approaches based on the prediction of a regularizer achieves superior quality of image reconstruction and beats the solutions that rely either on deep learning or on the optimization schemes alone. Finally, several proposed algorithms demonstrate low computational complexity, without sacrificing the accuracy of image restoration. Being fast and accurate, the proposed framework paves the way towards the real-time image restoration microscopy in low photon count conditions.

References

- [1] Diffraction psf 3d. <https://www.optinav.info/Diffraction-PSF-3D.htm>. Accessed: 2019-05-30. 5

- [2] Introduction to variational image-processing models and applications. *Int. J. Comput. Math.*, 90:1–8, 2013. 1
- [3] Yousef Al-Kofahi, Alla Borisovna Zaltsman, Robert Graves, Will Marshall, and Mirabela Rusu. A deep learning-based algorithm for 2-d cell segmentation in microscopy images. In *BMC Bioinformatics*, 2018. 5
- [4] Iman Hussein AL-Qinani. Deblurring image and removing noise from medical images for cancerous diseases using a wiener filter. *IRJET*, 8(4):2354–2365, 2017. 2
- [5] Francis John Anscombe. The transformation of poisson, binomial and negative-binomial data. 1948. 3
- [6] Dimitri P. Bertsekas. *Nonlinear programming: Second edition*. 1999. 5
- [7] Ajay Kumar Boyat and Brijendra Kumar Joshi. Image denoising using wavelet transform and wiener filter based on log energy distribution over poisson-gaussian noise model. *2014 IEEE International Conference on Computational Intelligence and Computing Research*, pages 1–6, 2014. 2
- [8] Antoni Buades, Bartomeu Coll, and Jean-Michel Morel. A non-local algorithm for image denoising. *2005 IEEE Computer Society Conference on Computer Vision and Pattern Recognition (CVPR'05)*, 2:60–65 vol. 2, 2005. 1
- [9] Mikael Carlavan and Laure Blanc-Féraud. Sparse poisson noisy image deblurring. *IEEE Transactions on Image Processing*, 21:1834–1846, 2012. 2
- [10] Dai-Qiang Chen. Regularized generalized inverse accelerating linearized alternating minimization algorithm for frame-based poissonian image deblurring. *SIAM J. Imaging Sciences*, 7:716–739, 2014. 2, 6, 7, 8
- [11] Aritra Chowdhury, Dmitry V. Dylvov, Qing Li, Michael MacDonald, Dan E. Meyer, Michael Marino, and Alberto Santamaria-Pang. Blood vessel characterization using virtual 3D models and convolutional neural networks in fluorescence microscopy. In *2017 IEEE 14th International Symposium on Biomedical Imaging (ISBI 2017)*, pages 629–632. IEEE, apr 2017. 2
- [12] José-Angel Conchello and Jeff William Lichtman. Fluorescence microscopy. *Nature Methods*, 2(12):910–919, 2005. 1
- [13] Jacques Boutet de Monvel, Sophie Le Calvez, and Mats Ulfendahl. Image restoration for confocal microscopy: improving the limits of deconvolution, with application to the visualization of the mammalian hearing organ. *Biophysical journal*, 80 5:2455–70, 2001. 1
- [14] Nicolas Dey, Laure Blanc-Féraud, Christophe Zimmer, Pascal Roux, Zvi Kam, Jean-Christophe Olivo-Marin, and Josiane Zerubia. Richardson-lucy algorithm with total variation regularization for 3d confocal microscope deconvolution. *Microscopy research and technique*, 69 4:260–6, 2006. 2, 3, 6, 7
- [15] David Eigen, Dilip Krishnan, and Rob Fergus. Restoring an image taken through a window covered with dirt or rain. *2013 IEEE International Conference on Computer Vision*, pages 633–640, 2013. 2
- [16] Valtere Evangelista, Laura Barsanti, Vincenzo Passarelli, and Paolo Gualtieri. From cells to proteins: Imaging nature across dimensions. 2005. 1
- [17] Mário A. T. Figueiredo and José M. Bioucas-Dias. Restoration of poissonian images using alternating direction optimization. *IEEE Transactions on Image Processing*, 19:3133–3145, 2010. 2, 6, 7, 8
- [18] Alessandro Foi, Mejd Trimeche, Vladimir Katkovnik, and Karen O. Egiazarian. Practical poissonian-gaussian noise modeling and fitting for single-image raw-data. *IEEE Transactions on Image Processing*, 17:1737–1754, 2008. 2
- [19] Thomas Kailath et al. *Linear least-squares estimation*. 2
- [20] Filippos Kokkinos and Stamatios Lefkimmiatis. Deep image demosaicking using a cascade of convolutional residual denoising networks. In *ECCV*, 2018. 1
- [21] F. Kokkinos and S. Lefkimmiatis. Iterative joint image demosaicking and denoising using a residual denoising network. *IEEE Transactions on Image Processing*, 28(8):4177–4188, Aug 2019. 2
- [22] Dilip Krishnan and Rob Fergus. Fast image deconvolution using hyper-laplacian priors. In *NIPS*, 2009. 1, 3
- [23] Jakob Kruse, Carsten Rother, and Uwe Schmidt. Learning to push the limits of efficient fft-based image deconvolution. *2017 IEEE International Conference on Computer Vision (ICCV)*, pages 4596–4604, 2017. 1, 2, 8
- [24] Martin Laasmaa, Marko Vendelin, and P. Peterson. Application of regularized richardson-lucy algorithm for deconvolution of confocal microscopy images. 2011. 2
- [25] S. Lefkimmiatis. Non-local color image denoising with convolutional neural networks. In *The IEEE Conference on Computer Vision and Pattern Recognition (CVPR)*, July 2017. 1
- [26] S. Lefkimmiatis. Universal denoising networks: A novel cnn architecture for image denoising. In *The IEEE Conference on Computer Vision and Pattern Recognition (CVPR)*, June 2018. 1
- [27] Stamatios Lefkimmiatis and Michael Unser. Poisson image reconstruction with Hessian Schatten-norm regularization. *IEEE Transactions on Image Processing*, 22:4314–4327, 2013. 2, 6, 7, 8
- [28] Jizhou Li, Florian Luisier, and Thierry Blu. Pure-let image deconvolution. *IEEE Transactions on Image Processing*, 27:92–105, 2018. 2, 6, 7, 8
- [29] Po-Yu Liu and Edmund Y. Lam. Image reconstruction using deep learning. *ArXiv*, abs/1809.10410, 2018. 2
- [30] Hongbing Lu, Jui-His Cheng, Guoping Han, Lihong Li, and Zhengrong Liang. 3d distance-weighted wiener filter for poisson noise reduction in sinogram space for spect imaging. 2001. 2
- [31] L. B. Lucy. An iterative technique for the rectification of observed distributions. 1974. 2
- [32] Xiao-Guang Lv, Le Jiang, and Jun Liu. Deblurring poisson noisy images by total variation with overlapping group sparsity. *Applied Mathematics and Computation*, 289:132–148, 2016. 2
- [33] Markku Mäkitalo and Alessandro Foi. A closed-form approximation of the exact unbiased inverse of the anscombe variance-stabilizing transformation. *IEEE Transactions on Image Processing*, 20:2697–2698, 2011. 3

- [34] Markku Mäkitalo and Alessandro Foi. Optimal inversion of the generalized anscombe transformation for poisson-gaussian noise. *IEEE Transactions on Image Processing*, 22:91–103, 2013. [2](#)
- [35] Ben Mildenhall, Jonathan T. Barron, Jiawen Chen, Dillon Sharlet, Ren Ng, and Robert Carroll. Burst denoising with kernel prediction networks. *2018 IEEE/CVF Conference on Computer Vision and Pattern Recognition*, pages 2502–2510, 2017. [1](#), [2](#), [4](#)
- [36] Messinger Anirudh Patel. Non-blind image deblurring using neural networks andy gilbert shai. 2018. [2](#)
- [37] Moacir Ponti, Elias Salomão Helou Neto, Paulo Jorge S. G. Ferreira, and Nelson D. A. Mascarenhas. Image restoration using gradient iteration and constraints for band extrapolation. *IEEE Journal of Selected Topics in Signal Processing*, 10:71–80, 2016. [2](#)
- [38] William Hadley Richardson. Bayesian-based iterative method of image restoration*. 1972. [2](#)
- [39] Leonid I Rudin, Stanley Osher, and Emad Fatemi. Nonlinear total variation based noise removal algorithms. *Physica D: nonlinear phenomena*, 60(1-4):259–268, 1992. [3](#)
- [40] Daniel Sage, Laurène Donati, Ferréol Soulez, Denis Fortun, Guillaume Schmit, Arne Seitz, R Guiet, Cédric Vonesch, and Michael A. Unser. Deconvolutionlab2: An open-source software for deconvolution microscopy. *Methods*, 115:28–41, 2017. [7](#), [8](#)
- [41] Uwe Schmidt and Stefan Roth. Shrinkage fields for effective image restoration. *2014 IEEE Conference on Computer Vision and Pattern Recognition*, pages 2774–2781, 2014. [1](#)
- [42] Colin J. R. Sheppard and T. Wilson. Image formation in confocal scanning microscopes. 1980. [1](#)
- [43] Jonathan R Shewchuk. An introduction to the conjugate gradient method without the agonizing pain. Technical report, Pittsburgh, PA, USA, 1994. [5](#)
- [44] Xin Tao, Hongyun Gao, Renjie Liao, Jue Wang, and Jiaya Jia. Detail-revealing deep video super-resolution. *2017 IEEE International Conference on Computer Vision (ICCV)*, pages 4482–4490, 2017. [1](#), [2](#)
- [45] A. N. Tikhonov. Solution of incorrectly formulated problems and the regularization method. *Soviet Math. Dokl.*, 4:1035–1038, 1963. [3](#)
- [46] Dmitry Ulyanov, Andrea Vedaldi, and Victor S. Lempitsky. Instance normalization: The missing ingredient for fast stylization. *ArXiv*, abs/1607.08022, 2016. [4](#)
- [47] Hongbin Wang and Paul C. Miller. Scaled heavy-ball acceleration of the richardson-lucy algorithm for 3d microscopy image restoration. *IEEE Transactions on Image Processing*, 23:848–854, 2014. [2](#)
- [48] Norbert Wiener. The extrapolation, interpolation and smoothing of stationary time series, with engineering applications. 1949. [2](#)
- [49] Li Xu, Jimmy S. J. Ren, Ce Liu, and Jiaya Jia. Deep convolutional neural network for image deconvolution. In *NIPS*, 2014. [2](#)
- [50] Jiawei Zhang, Jin shan Pan, Wei-Sheng Lai, Rynson W. H. Lau, and Ming-Hsuan Yang. Learning fully convolutional networks for iterative non-blind deconvolution. *2017 IEEE Conference on Computer Vision and Pattern Recognition (CVPR)*, pages 6969–6977, 2016. [1](#), [8](#)
- [51] Kai Zhang, Wangmeng Zuo, Shuhang Gu, and Lei Zhang. Learning deep cnn denoiser prior for image restoration. *2017 IEEE Conference on Computer Vision and Pattern Recognition (CVPR)*, pages 2808–2817, 2017. [1](#), [7](#), [8](#)
- [52] Xiaobo Zhang. An effective sure-based wiener filter for image denoising. In *ICC 2016*, 2016. [2](#)
- [53] Yide Zhang, Yin hao Zhu, Evan Nichols, Qingfei Wang, Siyuan Zhang, Cody Smith, and Scott Howard. A poisson-gaussian denoising dataset with real fluorescence microscopy images. In *The IEEE Conference on Computer Vision and Pattern Recognition (CVPR)*, June 2019. [2](#), [5](#)